THE JOURNAL OF PHYSICAL CHEMISTRY B LETTERS

2005, *109,* 7597−7600
Published on Web 04/05/2005

XPS Characterization of Au (Core)/SiO_2 (Shell) Nanoparticles

Ilknur Tunc and Sefik Suzer*

Chemistry Department and the Laboratory for Advanced Functional Materials, Bilkent University, 06800 Ankara, Turkey

Miguel A. Correa-Duarte and Luis M. Liz-Marzán

Departamento de Química Física, Universidade de Vigo, 36310 Vigo, Spain

Received: February 13, 2005; In Final Form: March 12, 2005

Core−shell nanoparticles with ca. 15-nm gold core and 6-nm silica shell were prepared and characterized by XPS. The Au/Si atomic ratio determined by XPS is independent of the electron takeoff angle because of the concentric spherical shape of the nanoparticles. The formula given by Wertheim and DiCenzo (*Phys. Rev. B* **1988**, *37*, 844) for spherical nanoparticles and the modified one by Yang et. al. (*J. Appl. Phys*. **2005**, *97*, 024303) for core−shell nanoparticles are used to correlate the XPS-derived composition with the geometry of the nanoparticles only after significantly modifying either the bulk density of the silica shell or the attenuation length of the photoelectrons.

Introduction

The race for production of nanoparticles with well-defined structures and tailored properties is still in its peak, because it is envisaged that they will revolutionize both our understanding and production of advanced materials soon.[1−11] Core−shell type of nanostructures particularly have a central place, because they offer extra stability and multifunctionality.[12−20] Among the analytical techniques for the characterization of core−shell-type nanostructures, X-ray photoelectron spectroscopy (XPS) is vital because of the perfect match of its probe length (∼10 nm) to the size of these particles and its ability to probe the chemical identity of the elements present.[21] Various reports have been published dealing with the use of XPS for characterization of various core−shell-type naostructures.[22−33]

When these core−shell nanoparticles are deposited on smooth surfaces for XPS analysis, the photoelectrons created are severely attenuated as they pass through the core and the shell before they escape into the vacuum for their kinetic energy analysis. This attenuation is, in principle, well-known and can be modeled to extract structural and morphological information from the XPS data. Wertheim and DiCenzo were the first to derive a formula relating the intensity of photoemission from spherical clusters.[22] Hoener et al. used the relative attenuation of primary photoelectrons and Auger signals to demonstrate the formation of a core−shell type of structure.[23] Katari, Colvin, and Alivisatos by use of XPS determined the surface composition of semiconductor nanocrystals.[24] In the paper by Dabbousi et al., XPS, together with other X-ray techniques, was utilized to determine chemical composition, size, shape, and internal structure of core−shell quantum dots.[25] Cao and Banin used XPS to provide direct proof that shells grow on core nanoparticles,[26] while Liu et al. claimed that XPS provided the direct proof of the core−shell structure of shell cross-linked micelles.[27] Koktysh et al.[28] used XPS to analyze silver/TiO_2 core−shell nanoparticle films before and after removing the silver core, and similar studies were used by Liu and Chuang on gold/polypyrrole core−shell nanocomposites.[29] Boyen et al. utilized angle-resolved XPS to estimate the size of the oxidation-resistant gold-55 clusters.[30] Yang et al. also used XPS intensities and/or their angle dependency to estimate the size and structure of Cu clusters on various surfaces.[31,32] In a very recent paper, the same group extended the formula, derived for a simple spherical particle by Wertheim and DiCenzo, for application to particles with a spherical core and a uniform shell and studied the oxidation kinetics of Si nanoparticles by XPS.[33] In most of the previous reports, only one element was probed by XPS to extract information about the structure of the core−shell nanoparticles. It is, however, desirable to probe by XPS different elements belonging to the core and the shell separately in order to extract more complete structural information, which eliminates many of the experimental sources of error. In this contribution, we report such a case where Au (core)/SiO_2 (shell) nanoparticles with a well-defined and characterized structure are analyzed by XPS, and we address issues related with angle dependency and escape depths usable for these nanostructures.

Experimental Details

Tetrachloroauric acid ($HAuCl_4 \cdot 3H_2O$), 3-aminopropyl trimethoxysilane (APS), and sodium silicate solution ($Na_2O(SiO_2)_{3-5}$, 27 wt % SiO_2) were purchased from Aldrich. Au/SiO_2 nanoparticles were prepared using the method described earlier.[13] Briefly, spherical gold nanoparticles with an average diameter of ca. 15 nm and 10% polydispersity were prepared by boiling 5×10^{-4} M $HAuCl_4$ in the presence of 1.6×10^{-3} M sodium citrate for 15 min. Upon cooling to room temperature, APS (5 μM) and sodium silicate solution (0.01 wt %) were

* Corresponding author: suzer@fen.bilkent.edu.tr.

10.1021/jp050767j CCC: $30.25 © 2005 American Chemical Society

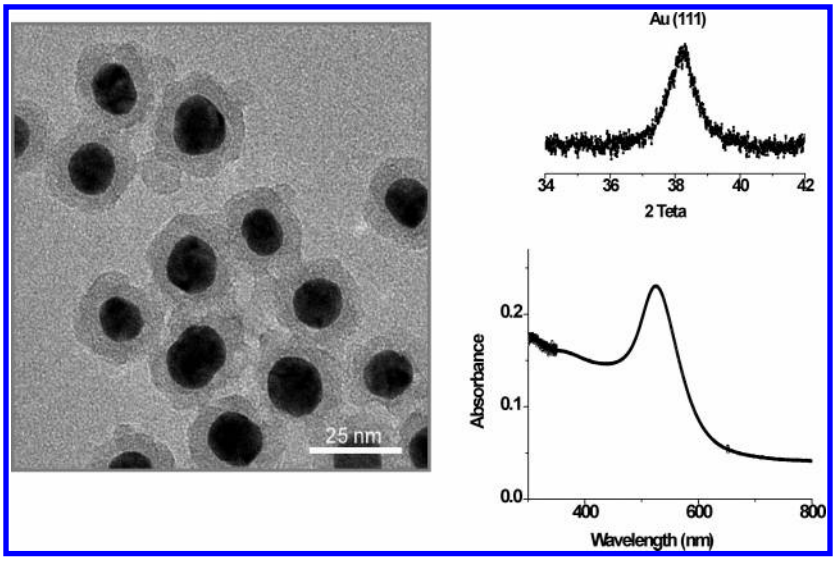

Figure 1. TEM image of the Au (core)/SiO_2 (shell) nanoparticles together with their X-ray diffraction pattern and the UV−vis absorption spectrum.

added in turn, under vigorous magnetic stirring. The resulting dispersion (pH ≈ 8.5) was allowed to stand for 3 days, resulting in the deposition of 5−7-nm-thick silica shells.

The nanoparticles were deposited on a copper tape and analyzed after drying in air using a Kratos ES300 electron spectrometer with Mg Kα X-rays. The UV−vis spectrum and the XRD pattern were recorded using a Cary 5E spectrometer and Rikagu Miniflex diffractometer with Cu X-rays, respectively. For comparison, gold was also deposited by plasma vapor deposition (PVD) on a silicon substrate containing ca. 4-nm oxide layer grown thermally. Standard curve-fitting procedures were employed to extract intensities of the peaks from their areas.

Results and Discussion

Figure 1 shows a representative transmission electron microscopy (TEM) image of the nanoparticles with an average diameter of 15-nm gold core and ca. 6-nm-thick silica shell. The UV−vis spectrum of the nanoparticles in aqueous solution and the XRD pattern are also shown in the same figure. The strong surface plasmon resonance band of the gold nanoparticles around 530 nm and the slightly broad ($\Delta\Phi > 0.8°$) XRD peak at 38°, corresponding to Au(111), are indicative of the crystalline gold core, and the only (indirect) evidence of the silica shell is revealed through the slight red-shift of the plasmon band with respect to the citrate−gold colloid, as has been previously discussed.[13]

Figure 2a displays the XPS spectrum of the region corresponding to the binding energy range of 110−70 eV, which includes the Si 2p, Au 4f, and Cu 3p peaks recorded at 90° and 30° electron takeoff angles, respectively. Chemical identity of the elements (determined from the measured binding energies) is straightforward and corresponds to Au^0 and Si^{IV}.

To gain more information about the composition, the Si Auger parameter and angle-dependent atomic ratios are determined. These are compared to the case of gold clusters deposited from the vapor phase onto a silicon surface containing a ca. 4-nm oxide layer, the spectra of which at the two takeoff angles are also reproduced in Figure 2b. The silicon Auger parameter, which is defined as the sum of the Si 2p binding energy and the Si_{KLL} kinetic energy of the sample under investigation is a better indicator of the chemical identity, because it is insensitive to charging and other experimental artifacts.[34−36] In the case of

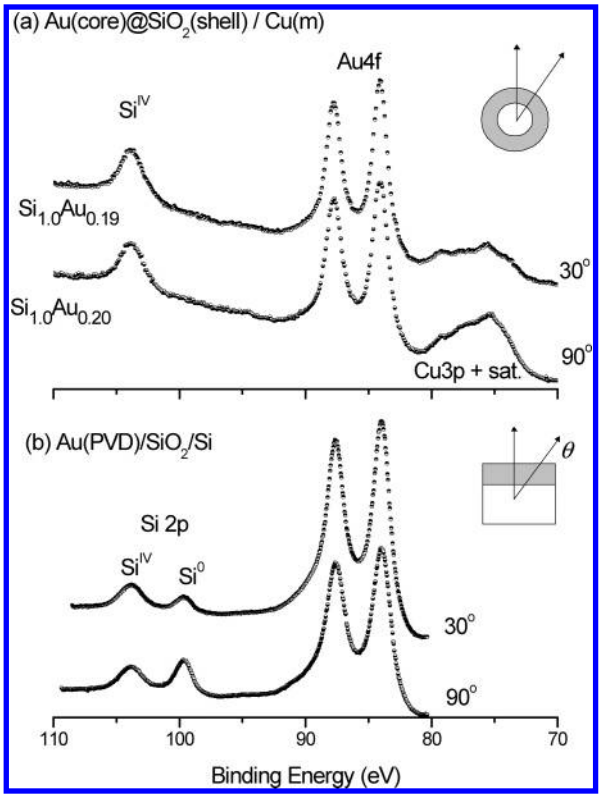

Figure 2. The 110−70 eV region of the XPS spectrum recorded at 90° and 30° electron takeoff angles corresponding to (a) Au (core)/SiO_2 (shell) nanoparticles deposited on copper tape, (b) gold particles vapor-deposited (PVD) onto a silicon substrate containing ca. 4-nm oxide layer.

the gold (core)−silica (shell) nanoclusters, the Auger parameter of the silicon atom was determined to be 1711.8 eV, which is very close to that of the silicon oxide layer as given in Table 1.

The Au 4f peak appears quite strong because of its higher photoionization cross-section (17.47) compared to that of Si 2p (0.865). The atomic ratios determined by XPS, after correction for atomic cross-sections, at different electron takeoff angles for the core−shell nanoclusters are shown in Figure 2a and Figure 3 together with the case when gold is deposited from the vapor phase on the SiO_2/Si system. When the XPS spectrum of a heterogeneous sample is recorded at a lower electron takeoff angle, the relative intensity of the peaks of the elements near

TABLE 1: Measured Binding and Kinetic Energies of the Si 2p and Si_{KLL} Peaks and the Derived Auger Parameter for the Au (Core)/SiO_2 (Shell) Nanoparticles[a]

	Si 2p BE (eV)		Si_{KLL} KE (eV)		α (eV)	
	Si^{IV}	Si^0	Si^{IV}	Si^0	Si^{IV}	Si^0
C−S	103.3		1608.5		1711.8	
SiO_2/Si	103.9	99.5[b]	1608.1	1616.4[b]	1712.0	1715.9

[a] The same data for a ca. 4-nm thermally grown SiO_2/Si system are given for comparison. [b] Taken as the reference.

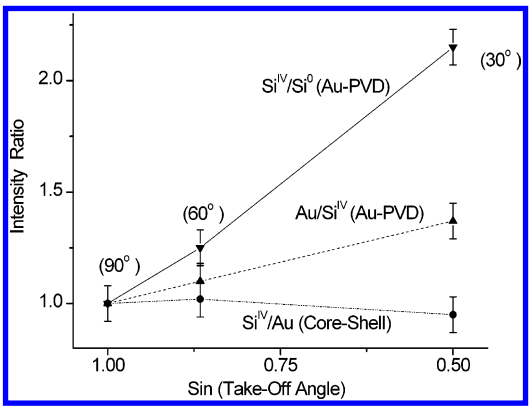

Figure 3. Intensity ratio of XPS peaks for $Si(2p)^{IV}/Si(2p)^0$ and Au $4f/Si(2p)^0$ from the PVD sample and Au $4f/Si(2p)^{IV}$ from the Au/SiO_2 sample, at three different takeoff angles, normalized to the ratio at 90°, and plotted against the sine of the angle.

the surface increases at the expense of the peaks away from the surface. Accordingly, for the sample where gold is vapor-deposited on the silicon substrate, which also contains a ca. 4-nm thermally grown oxide layer, the intensity of the Si 2p peak belonging to the oxide (Si^{IV}) increases, and that of the silicon (Si^0) decreases at 30°. Similarly, the Au 4f peak intensity increases at the expense of both of the silicon peaks, because it is the outermost surface species. In the case of the core−shell nanoclusters, the intensity of the Si 2p and Au 4f peaks increases with respect to the Cu 3p substrate peak at the lower takeoff angles; however, the Au/Si atomic ratio stays constant within the experimental uncertainty limits. A similar case was reported and discussed in detail by Piyakis et al. in the analysis of spherical Cu nanoclusters, by using angle-resolved XPS; and by performing Monte Carlo simulation, they showed that, if the radius of the particle is larger than the attenuation length of the photoelectron, the intensity is more or less angle-independent.[32] Our finding that the ratio of the intensity of the XPS peak of the element stemming from the core to that from the shell is also angle-independent not only supports their findings but also extends it to core−shell nanoclusters.

To relate the XPS-determined composition to the geometry of the core−shell nanoclusters, one has to take into account the attenuation of the photoelectrons as they traverse the core and the shell, as well as the density of the Si atoms (0.0383 mol/cm^3 obtained from the bulk density of the silicon dioxide, 2.3 g/cm^3) in the shell and the Au atoms (0.0980 mol/cm^3 obtained from the bulk density of gold, 19.3 g/cm^3) in the core.

Attenuation of photoelectron intensity is given by the formula, $I = I_0(e^{-d/\lambda})$, as the photoelectrons traverse a medium with a finite thickness d, where λ is the attenuation length (or the escape depth), which depends strongly on the kinetic energy of the photoelectrons and also on the density of the medium.[36] The kinetic energies of the Au 4f and Si 2p photoelectrons are very close to each other; hence, the first factor does not need to be considered in this case. However, the densities of the gold core and the silica shell, and also their scattering powers, need to be taken into account. In the formula derived by Wertheim and Dicenzo,[21] the intensity of a photoelectron peak from a spherical cluster is given by

$$S = \pi\lambda^3\{x^2 + [(2x+1)e^{-2x} - 1]/2\} \quad (1)$$

where λ is the photoelectron's attenuation length and $x = r/\lambda$, with r being the radius of the cluster. This formula can be adopted for calculation of the intensity of the concentric silica shell by first taking the radius as 13.5 nm (sum of the core radius and the shell thickness) and 7.5 nm (core radius) separately, and then taking the difference. However, for the gold core, we have to take into account the attenuation through the silica shell. One way is to use a simple attenuation factor through the shell

$$S(\text{core}) = e^{-d/\lambda S} \times \pi\lambda_C{}^3\{x^2 + [(2x+1)e^{-2x} - 1]/2\} \quad (2)$$

where d is the thickness of the silica shell and λ_S and λ_C are the attenuation lengths of the core and the shell, respectively. The extended formula derived by Yang et al.[33] is similar to eq 2 but also includes additional terms

$$S(\text{core}) = \{[\kappa(x)d + \lambda]/(d + \lambda)\} \times e^{-d/\lambda}{}_* \pi\lambda^3\{x^2 + [(2x+1)e^{-2x} - 1]/2\} \quad (3)$$

where $\kappa(x)$ is another function containing several other terms. Two points are relevant to our discussion below: (i) the additional term in eq 3 is always smaller than 1, and (ii) eq 3 yields eq 1 when $d = 0$. Another important point is that in deriving their equation Yang et al.[33] used a single attenuation length for the core and the shell, which we think is not appropriate for our case.

Practical attenuation lengths with Mg Kα X-rays for the Au 4f peak in the gold metal and the Si 2p peak in the silicon oxide are given as 1.44 and 2.74 nm, respectively.[37] If we use eq 2 for gold attenuation through the silica shell ($e^{-6.0/2.74} = 0.112$). we obtain 0.07 for the Au/Si atomic ratio, which is too low as compared with the experimental value of 0.20. Using eq 3 leads to an even lower atomic ratio of 0.05.

Assuming that the TEM data are reliable, we state the following as contributing to the larger than predicted Au/Si ratio:

(i) In addition to core−shell nanoparticles, there exist extra gold particles either without silica shells or with silica shells thinner than 6 nm.

(ii) The silica shell is less dense, resulting in a smaller concentration.

(iii) The attenuation lengths are different (larger than) from their bulk values.

The first point can be ruled out because of our additional observation (not shown here) that both the Si 2p and Au 4f peaks undergo similar differential charging, indicating that they are within close proximity and leading to the conclusion that just one kind of gold species is present. This issue will be discussed in more detail in a forthcoming publication.[36,38] The second point is a more likely contribution, because the silica shell was prepared through the precipitation of sodium silicate from solution, and oligomers form in solution prior to the aggregation and could also get incorporated. Therefore, the porosity achieved is rather high, and even higher than for organosilica, as was demonstrated by studying chemical reactions on metal cores.[39] On the other hand, though the thickness of the silica shells is rather uniform, from TEM we can also see some cases with thinner shells or shells with less uniform thickness, which may influence through the first point. As for

TABLE 2: Calculated Au/Si Atomic Ratio for the Au (Core)/Silica (Shell) Nanoparticles Using Different Parameters by XPS Together with the Experimentally Determined Ratio

	λ-core (nm)	λ-shell (nm)	shell density (mol/cm^3)	Au/Si ratio	
experimental				0.20	
calculated				eq 2	eq 3
	1.44	2.74	0.0383	0.07	0.05
	1.44	3.50	0.0383	0.08	0.06
	1.44	3.50	0.0200	0.16	0.12
	1.44	3.50	0.0160	0.20	0.16
	2.50	3.50	0.0270	0.20	0.18
	3.50	3.50	0.0383	0.19	0.14
	3.50	3.50	0.0270	0.27	0.20

the gold core, we must use the metallic density because of the observation of the Au(111) diffraction peak. The third point is also closely related to the second one, because density is an important parameter contributing to the attenuation of the photoelectrons. Along these lines, Yang et al. used the attenuation length of 3.5 nm for the silicon oxide layer for relating their XPS intensities to the silicon oxide−silicon core−shell nanoparticles and questioned the use of bulk densities for nanoparticles.[33] Accordingly, we have calculated a number of possible cases using different values for the densities and attenuation lengths as given in Table 2 using both eqs 2 and 3. From the analysis of the data in the table, we see that, irrespective of the equation we use, we can reproduce the experimentally derived Au/Si atomic ratio only after drastically reducing the density of the silica layer. Obviously, other combinations can also be found for the corresponding attenuation length and density to match the experimental ratio, which calls for further experimental and theoretical work.

Conclusions

Two important conclusions can be drawn from this work. First, the XPS intensity ratio of peaks from elements of the core and the shell is independent of the electron takeoff angle, which, we think, is an important tool for extracting geometrical information about nanoparticles. Second, for elucidating the composition, size, geometry, and so forth of nanoparticles from XPS measurements, bulk data are not reliable. Hence, (i) new approaches for modifying the bulk data and (ii) a new mathematical model taking into account different attenuation through the core and the shell must be developed.

Acknowledgment. This work was partially supported by TUBA (Turkish Academy of Sciences) and MEC (Ministerio de Educación y Ciencia, Spain).

References and Notes

(1) Henglein, A. *Chem. Rev.* **1989**, *89*, 1861.
(2) Stucy, G. D.; MacDougall *Science* **1990**, *247*, 669.
(3) Alivisatos, A. P. *Science* **1996**, *271*, 2693.
(4) Grieve, K.; Mulvaney, P.; Grieser, F. *Curr. Opin. Colloid Interface Sci.* **2000**, *5*, 168.
(5) Shipway, A. N.; Katz, E.; Willner, I. *Chem. Phys. Chem.* **2000**, *1*, 18.
(6) Lue, J. T. *J. Phys. Chem. Solids* **2001**, *62*, 1599.
(7) Tempelton, A. C.; Wuelfing, W. P.; Murray, R. W. *Acc. Chem. Res.* **2000**, *33*, 27.
(8) Trindade, T.; O'Brien, P.; Pickett, N. L. *Chem. Mater.* **2001**, *13*, 3843.
(9) Brust, M.; Kiely, C. J. *Colloids Surf., A* **2002**, *202*, 175.
(10) Kamat, P. V. *J. Phys. Chem. B* **2002**, *106*, 7729.
(11) El-Sayed, M. A. *Acc. Chem. Res.* **2004**, *37*, 326.
(12) Chen, M. S.; Goodman, D. W. *Science* **2004**, *306*, 252.
(13) Liz-Marzán, L. M.; Giersig, M.; Mulvaney, P. *Langmuir* **1996**, *12*, 4329.
(14) Liz-Marzán, L. M.; Mulvaney, P. *J. Phys. Chem. B* **2003**, *107*, 7312.
(15) Hardikar, V. V.; Matijevic, E. J. *J. Colloid Interface Sci.* **2000**, *221*, 133.
(16) Hodak, J. H.; Henglein, A.; Hartland, G. V. *J. Chem. Phys.* **2001**, *114*, 2760.
(17) Caruso, F. *Adv. Mater.* **2001**, *13*, 11.
(18) Schierhorn, M.; Liz-Marzan, L. *Nano Lett.* **2002**, *2*, 13.
(19) Liu, Y.; Yin, Y.; Xia, Y. *Nano Lett.* **2002**, *2*, 785.
(20) Salgueirino-Maceira, V.; Caruso, F.; Liz-Marzan, L. *J. Phys. Chem.* **2003**, *107*, 10990.
(21) Briggs, D.; Seah, M. P. *Practical Surface Analysis*, 2nd ed.; Wiley: Chichester, U.K., 1999; Vol. I.
(22) Wertheim, G. K.; DiCenzo, S. B. *Phys. Rev. B* **1988**, *37*, 844.
(23) Hoener, C. F.; Allan, K. A.; Bard, A. J.; Campion, A.; Fox, M. A.; Mallouk, T. E.; Webber, S. E.; White, J. M. *J. Phys. Chem.* **1992**, *96*, 3812.
(24) Katari, J. E. B.; Colvin, V. L.; Alivisatos, A. P. *J. Phys. Chem.* **1994**, *98*, 4109.
(25) Dabbousi, B. O.; Rodriguez-Viejo, J.; Mikulec, F. V.; Heine, J. R.; Mattoussi, H.; Ober, R.; Jensen, K. F.; Bawendi, M. G. *J. Phys. Chem. B* **1997**, *101*, 9463.
(26) Cao, Y. W.; Banin, U. *J. Am. Chem. Soc.* **2000**, *122*, 9692.
(27) Liu, S.; Ma, Y.; Armes, S. P.; Perruchot, C.; Watts, J. F. *Langmuir* **2002**, *18*, 7780.
(28) Koktysh, D. S.; Liang, X.; Yun, B. G.; Pastoriza-Santos, I.; Matts, R. L.; Giersig, M.; Serra-Rodríguez, C.; Liz-Marzán, L. M.; Kotov, N. A. *Adv. Funct. Mater.* **2002**, *12*, 255.
(29) Liu, Y.-C.; Chuang, T. C. *J. Phys. Chem. B* **2003**, *107*, 9692.
(30) Boyen, H. G.; Kastle, G.; Weigl, F.; Koslowski, B.; Dietrich, C.; Ziemann, P.; Spatz, J. P.; Riethmuller, S.; Hartmann, C.; Moller, M.; Schmid, G.; Garnier, M. G.; Oelhafen, P. *Science* **2002**, *297*, 1533.
(31) Yang, D.-Q.; Meunier, M.; Sacher, E. *J. Appl. Surf. Sci.* **2005**, *173*, 134.
(32) Piyakis, K. N.; Yang, D.-Q.; Sacher, E. *Surf. Sci.* **2003**, *536*, 139.
(33) Yang, D.-Q.; Gillet, J.-N.; Meunier, M.; Sacher, E. *J. Appl. Phys.* **2005,** *97*, 024303.
(34) Wagner, C. D. *Anal. Chem.* **1972**, *44*, 972.
(35) Baranco, A.; Yubera, F. Espinos, J. P.; Elippe, A. R. *Surf. Interface Anal.* **2001**, *31*, 761.
(36) Karadas, F.; Ertas, G.; Suzer, S. *J. Phys. Chem. B* **2004**, *108*, 1515.
(37) Jablonski, A.; Powell, C. J. *Surf. Sci.* **2002**, *520*, 78.
(38) Differential charging is frequently encountered in XPS analysis of poorly conducting samples and is considered a nuisance, but it can be turned into a useful analytical tool (Suzer, S. *Anal. Chem.* **2003**, *75*, 2939). For example, as we had demonstrated earlier, atoms within the same domain of a heterogeneous surface structure exhibit similar charging behavior as in the case of Au 4f and Si 2p peaks of the core−shell nanoparticles studied in this work.
(39) Ung, T.; Liz-Marzán, L. M.; Mulvaney, P. *Langmuir* **1998**, *14*, 3740.